

Cite this: *J. Mater. Chem. A*, 2019, 7, 18529

Integration of photoelectrochemical devices and luminescent solar concentrators based on giant quantum dots for highly stable hydrogen generation†

Guiju Liu,^a Baofen Sun,^b Hongliang Li,^b Yiqian Wang^{*a} and Haiguang Zhao^{ID} ^{*a}

Hydrogen generation from water under sunlight illumination is the key to construct a sustainable and clean energy system. To date, the long-term stability of photoanodes based on colloidal quantum dots (QDs) for hydrogen generation remains a major challenge due to the degradation of the QDs and hole accumulation. The degradation is usually caused by the self-oxidation of QDs induced by ultraviolet radiation. Here, we propose a concept of integrating a luminescent solar concentrator (LSC) with a photoelectrochemical (PEC) cell into a standalone device to improve the stability of the PEC device for hydrogen generation by avoiding direct irradiation of ultraviolet light on PEC devices. In this study, CdSe/(Cd_xSe_{1-x})₅/CdS core/multi-shell QDs were used as a photosensitizer. The PEC device based on alloyed multi-shell QDs shows a saturated photocurrent density of 11.5 mA cm⁻² and maintains ~16.2% of its initial value after 23 hours of sunlight illumination (100 mW cm⁻²). PEC devices based on QDs coupled with an LSC exhibit a saturated photocurrent density of 1.2 mA cm⁻², and ~84.6% of its initial value was retained after 23 hours of continuous illumination, indicating a 420% enhancement compared to a PEC device alone. This finding proves a unique concept to improve the photo-stability of PEC devices by coupling with an LSC.

Received 16th June 2019
Accepted 9th July 2019

DOI: 10.1039/c9ta06437k

rsc.li/materials-a

Introduction

Converting solar energy to other energy forms, like electricity, fuel, heat and chemical energy, can solve the current energy crisis, decrease our dependence on fossil fuels and reduce CO₂ emission and air pollution.¹⁻³ Among them, solar-driven hydrogen (H₂) generation is one of the efficient ways to solve the current challenges of renewable energy conversion and storage, because H₂ is a clean fuel with a high energy storage density and water is the only combustion byproduct.^{3,4} One of the most effective strategies for solar-to-H₂ energy conversion is photoelectrochemical (PEC) hydrogen production.^{5,6} Typically, a PEC device consists of a photoanode, a counter electrode, a reference electrode and an electrolyte. The PEC process can integrate the advantages of photocatalysis and electrocatalysis, which performs redox reactions driven by electron-hole pairs, leading to hole oxidation and electron movement to the counter electrode for H₂ generation.³ It can effectively collect H₂ and reduce the recombination rate of electrons and holes. In PEC devices, the solar-to-H₂ conversion efficiency and stability of H₂

evolution mainly depend on the performance of the photoanode. Usually, an ideal photoanode is composed of semiconductor materials, like oxides and oxide/quantum dots (QDs), with a suitable band structure, wide absorption spectrum and high photo-stability.

Recently, sensitizing wide band gap oxides with colloidal semiconducting QDs has been proven to be an efficient way to improve light absorption of the photoanode and further enhance the solar-to-H₂ conversion efficiency as the QDs can absorb sunlight in a wide spectral range, matching well with the solar spectrum.⁷⁻⁹ Until now, various types of oxide/QD systems (*e.g.* TiO₂/CdSe/CdS,¹⁰ TiO₂/PbS/CdS,¹¹ TiO₂/CdSe_xTe_{1-x}/CdS,¹² ZnO/CdS,¹³ NiO/CdSe¹⁴ and TiO₂/CdS¹⁵) have been used as light converters in PEC devices. The band gap and band energy levels of QDs can be well controlled by tuning their size/shape/composition. For example, by controlling the QD size, Li *et al.*¹⁶ reported size dependent electron transfer rates in Pt-decorated QDs, and obtained a higher H₂ generation quantum efficiency in small QDs (17.3% for 2.8 nm diameter *vs.* 11.4% for 4.6 nm diameter). By engineering the shell thickness of CdS/CdSe QDs, the photocatalytic H₂ evolution rate was 49% higher than that of the CdS core.¹⁷ So far, the highest saturated photocurrent density (*J*) of 22.1 mA cm⁻² was obtained for H₂ production in PEC devices based on PbS/Mn-doped CdS QDs.¹⁸ In practice, the efficiency, stability and cost of PEC devices are the key factors determining its application prospect. Compared to the largely

^aCollege of Physics, State Key Laboratory, Qingdao University, No. 308, Ningxia Road, Qingdao, 266071, P. R. China. E-mail: yqwang@qdu.edu.cn; hgzhao@qdu.edu.cn

^bCollege of Materials Science and Engineering, Qingdao University, No. 308, Ningxia Road, Qingdao, 266071, P. R. China

† Electronic supplementary information (ESI) available. See DOI: 10.1039/c9ta06437k

improved current density, the stability of PEC devices based on QDs is still a big challenge due to the influence of the stability of QDs.

Generally, QDs are sensitive to surface environments, such as a chemical environment (*e.g.* alkaline electrolyte environment) and light (especially ultraviolet (UV) light) which may lead to chemical- or photo-corrosion of the QDs, respectively. To decrease the influence of the chemical environment, using a neutral electrolyte may be a promising approach to enhance the stability of PEC devices. However, in a neutral electrolyte, hole oxidation is slow, so the solar-to-H₂ conversion efficiency in QD based PEC devices is low due to the fast e–h recombination. Meanwhile, self-oxidation would increase due to hole accumulation, resulting in the reduction of stability.¹⁹ At present, efforts to reduce photo/chemical-corrosion mainly focus on the performance improvement of the photoanode materials themselves. Considering that the stability of a PEC device is mainly determined by the charge separation efficiency, interfacial charge transfer rate and kinetics between electrons and holes, many researchers made efforts to develop highly efficient and long-term stable QDs to improve the performance of PEC devices.^{20–22} Among various kinds of QDs, “giant” core/shell QDs (with shell thickness >1.5 nm) provide an efficient approach to decrease the photocorrosion of QDs due to the thick shell, protecting the core of the QDs during the PEC process. However the thick shell could serve as an energy barrier to block efficient hole transfer. Because of hole accumulation, the self-oxidation of QDs often leads to the decrease of the H₂ generation efficiency.^{21,22} Recent efforts concentrate on engineering the interfacial structure of QDs to improve the stability and efficiency of PEC devices.^{7,9} For example, Bae *et al.*⁷ demonstrated that the introduction of an intermediate CdSe_xS_{1–x} layer between the CdSe core and CdS shell can improve the efficiency of the PEC device. Zhao *et al.*⁹ reported the improvement in the stability of PEC devices by using alloyed CdSe/Pb_xCd_{1–x}S/CdS QDs. Another promising approach to improve the stability of PEC devices is to decrease the UV effect (4%). Several methods were reported, such as using UV cutoff filters, doping with TiO₂ or replacing TiO₂ with UV inactive materials.^{13,23,24} However, the efficiency of the devices based on these approaches decreases due to the loss of UV light. A possible solution to avoid the damage of high energy photons on photoanodes and simultaneously use UV light is to convert UV light to other wavelengths of light that can be absorbed by the PEC devices.

Luminescent solar concentrators (LSCs) are large-area sunlight collectors. They consist of an optical waveguide embedded with down-shifting or up-converting fluorophores, which absorb sunlight and re-emit photons in a longer or shorter wavelength range.^{25–31} One of the efficient ways to avoid the UV effect is to design an integrated system of an LSC and a PEC device, which can be achieved by engineering the structure of QDs to match the LSC's emission with the absorption of QDs used for the photoanode. In this system, the performance of LSCs can affect the ultimate solar-to-H₂ efficiency and photo/chemical-stability. Up to now, the highest external optical efficiency (η_{opt} , defined as the ratio between the optical power of re-

emitted photons reaching the edges of an LSC and the optical power of incident photons) of LSCs based on nanomaterials has reached 26% ($10 \times 10 \text{ cm}^2$) using layered perovskite nanoplatelets.³² When η_{opt} of an LSC is high enough, theoretically, the LSC–PEC system can reduce the cost of H₂ production per molar mass, due to the much lower production cost of an LSC compared to a PEC device.³³ To the best of our knowledge, except the study by Cambié *et al.*³⁴ using LSC-photo-microreactors for photoredox catalysis, there is no report of PEC devices integrated with LSCs for H₂ production.

Here, we design a PEC device integrated with an LSC based on giant QDs for stable H₂ production. The PEC photoanode is placed at the edges of the LSC (as shown in Fig. 1a), and re-emitted light can be collected by the photoanode, where dissociation of the photogenerated excitons occurs, and electrons are injected into TiO₂ and then transferred to the Pt counter electrode to produce H₂. Na₂S and Na₂SO₃ hole scavengers in the electrolyte provide a shuttle for the photo-generated holes.¹¹ To make the utmost use of solar energy, the coupling of the LSC and PEC devices requires the emission spectrum of the LSC and the absorption spectrum of PEC photoanode to overlap as much as possible, as shown in Fig. 1b, so that the re-emitted light by the LSC can be absorbed by the photoanode. As a proof-of-concept, giant QDs with different shell compositions and thicknesses were chosen for the fabrication of the LSC–PEC system. The LSC was prepared by using “giant” CdSe/(CdS)₁₅ core/shell QDs (denoted as CdSe/CdS) with an emission peak at 624 nm and a full width at half maximum (FWHM) of 35 nm (Fig. 1b, red line). To absorb the re-emitted light from the LSC effectively, CdSe/(Cd_xSe_{1–x})₅/CdS core/multi-shell QDs (denoted as CdSe/CdSSe/CdS) with an alloyed interfacial layer were used to prepare the photoanode. The presence of the Cd_xSe_{1–x} interfacial layer largely improves the absorption range of the CdSe/CdS QDs, particularly in the range of 500–650 nm, matching very well with the PL spectrum of the CdSe/CdS QDs (Fig. 1b).

Results and discussion

To meet the requirements of the LSC–PEC system, the structure of the QDs was adjusted by controlling the shell layer thickness and chemical composition. Details of synthetic procedures for different QDs are shown in the ESI.† Fig. 2a and d show typical bright-field (BF) transmission electron microscope (TEM) images of the CdSe/CdS QDs and CdSe/CdSSe/CdS QDs with spherical morphology. Through the TEM images, we obtained the particle distribution and calculated the average diameter, as shown in Fig. S1.† The average diameters of the CdSe/CdS QDs and CdSe/CdSSe/CdS QDs are $12.1 \pm 3 \text{ nm}$ and $5.5 \pm 1.5 \text{ nm}$, respectively, indicating that the shell thicknesses are 4.4 nm and 1.0 nm after the growth of 15 monolayers of CdS or 5 monolayers of CdSSe and 1 monolayer of CdS, respectively. The CdSe core of the QDs has a zinc-blende (ZB) crystal structure (Fig. S2†), while the thermally stable phase of the CdS shell has a wurtzite (WZ) structure.³⁵ Thus, crystalline phase transformation may occur during the shell growth of the CdS shell on ZB CdSe cores *via* a successive ionic layer adsorption and

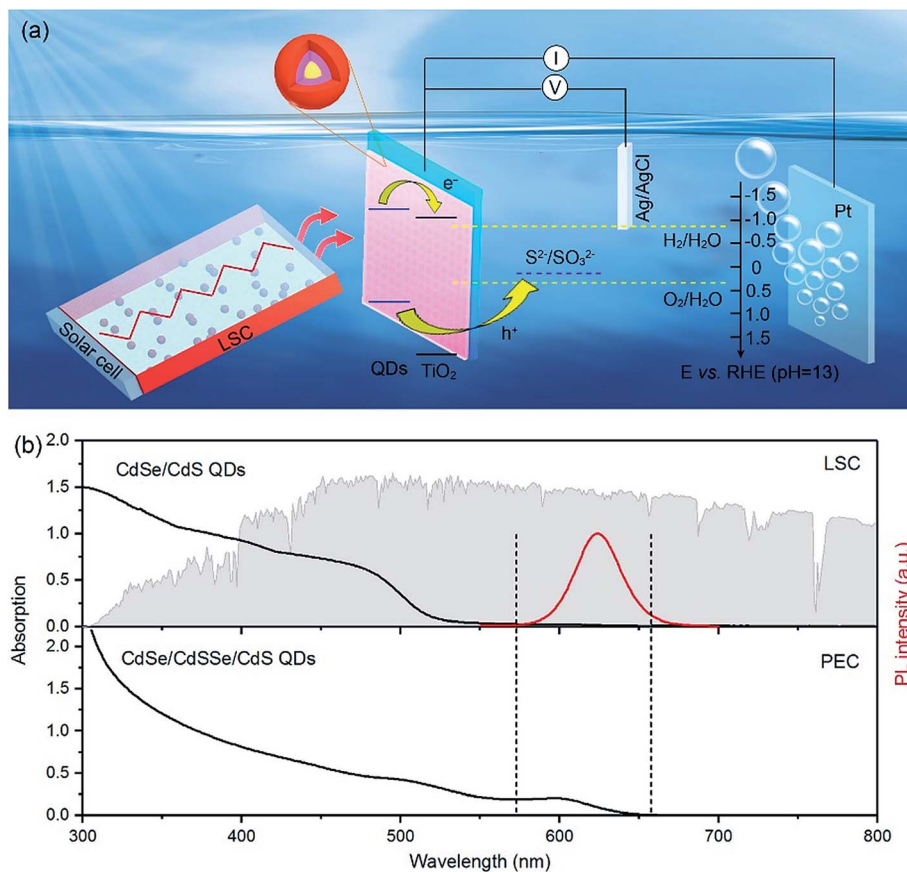


Fig. 1 (a) Band alignment and schematic diagram of the CdSe/CdSSe/CdS QD sensitized photoanode combined with a QD based LSC. The yellow arrows indicate the e–h transfer process. (b) Top: absorption and normalized PL spectra of the LSC based on CdSe/CdS QDs together with the AM 1.5G solar spectrum (grey shading). Bottom: the absorption spectrum of CdSe/CdSSe/CdS QDs used for the photoanode.

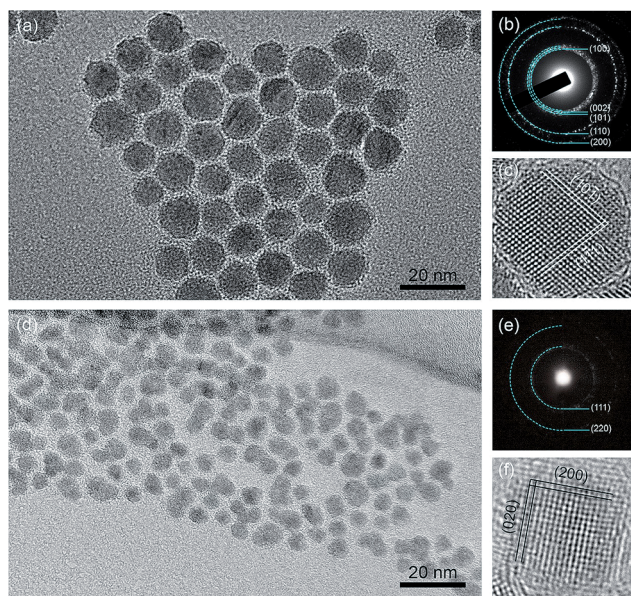


Fig. 2 (a–c) BF TEM, SAED and HRTEM images of the CdSe/CdS QDs, respectively. (d–f) BF TEM, SAED and HRTEM images of the CdSe/CdSSe/CdS QDs, respectively.

reaction (SILAR) approach. X-ray diffraction (XRD) patterns demonstrate that both types of QDs have two phase components: ZB and WZ (Fig. S2[†]). For the QDs with the 15-monolayer shell, the dominant phase is WZ, while for the QDs with the 6-monolayer shell the dominant phase is ZB, which is consistent with the selected-area electron diffraction (SAED) patterns (Fig. 2b and e) and high-resolution TEM (HRTEM) results (Fig. 2c and f). As shown in Fig. 2c, a lattice spacing of ~ 3.20 Å for the two planes with a crossing angle of 80° is measured, which is associated with the $(10\bar{1})$ and $(1\bar{1}1)$ planes of WZ CdS. The measured lattice spacing of ~ 2.92 Å for the two vertical planes in the HRTEM image in Fig. 2f corresponds to the (200) and (020) planes of the ZB CdSe phase. Energy dispersive X-ray spectroscopy (EDS) analysis confirms the presence of Cd, Se and S elements in these core/shell QDs (Fig. S3a and b[†]).

For the preparation of the photoanode, the CdSe/CdSSe/CdS QDs were deposited by electrophoretic deposition (EPD) on a TiO₂ mesoporous film (details in the Experimental section). Two coating cycles of ZnS layers were further applied by the SILAR method after EPD.¹⁷ After 1.5 h of the EPD process, the QDs were well dispersed on TiO₂ without noticeable aggregation (as shown in Fig. S4[†]), which contributes to the efficient electron transfer from QDs to TiO₂ in PEC devices. The EDS spectra in Fig. S3b and c[†] show the compositional evolution of the

CdSe/CdSSe/CdS QDs deposited on the TiO₂ mesoporous layer after two coating cycles of ZnS layers were applied on TiO₂/QDs.

For the preparation of the LSC, CdSe/CdS giant QDs as the emitter were embedded in a poly(lauryl methacrylate) (PLMA) polymer matrix (Experimental section). A 5 × 5 × 0.2 cm³ prototype LSC based on the CdSe/CdS QDs is presented in the inset in Fig. 3a. The ultra-thick shell can efficiently enhance the efficiency and photo-stability of the LSC as reported in the literature.²⁶ The solar-to-electrical power conversion efficiency (PCE) of the as-prepared LSC was measured by single-crystalline silicon solar cells. It is defined as the ratio of the output electric power of the solar cell coupled with the LSC and the input optical power:^{36,37}

$$\text{PCE} = \frac{I_{\text{sc}} \times V_{\text{oc}} \times \text{FF}}{P \times A_{\text{top}}} \quad (1)$$

where I_{sc} is the short circuit current, V_{oc} is the open circuit voltage, FF is the fill factor, P is the radiation intensity, and A_{top} is the top surface area of the LSC.

Another parameter to determine the optical performance of the LSC is η_{opt} which can be calculated using the following equation:³⁸

$$\eta_{\text{opt}} = \frac{P_{\text{out}}}{P_{\text{in}}} = \frac{I_{\text{out}}}{I_{\text{in}} \times G} \quad (2)$$

where P_{out} is the output power coming from the edges of the LSC and P_{in} is the input power on the top surface of the LSC. I_{out} and I_{in} are the corresponding output power density and input power density, respectively.

As shown in Fig. S5,† the PCE of a standalone solar cell and LSC-solar cell system is calculated to be ~12.0% and ~4.2%,

respectively. According to the two J - V curves, the η_{opt} of the LSC is calculated to be 5.4% using eqn (2). In an ideal situation, the LSC should be in contact with the photoanode as shown in Fig. S6a.† But in practice, the LSC is not in direct contact with the photoanode due to the geometry of the PEC cell. The LSC and PEC device are separated by an electrolytic tank (Fig. S6b†), which leads to the decrease of light intensity radiated to the photoanode. Under one sun illumination (100 mW cm⁻²), the short circuit current density of the solar cell is ~33 mA cm⁻². Through measuring the short circuit current density at the position of the photoanode, we can calculate the light intensity of the LSC radiating to the front side of the photoanode. In the H₂ production process, the light intensity on the edge of the LSC radiated to the photoanode is about 11.8 mW cm⁻² (Fig. 3a) under one sun illumination.

Fig. 3b shows the current density vs. applied potential (J - V) curves of the PEC devices in the dark and under the illumination of the LSC. The J of the LSC-PEC system is ~1.2 mA cm⁻² at ~0.6 V vs. the reversible hydrogen electrode (RHE), which is lower than that of the PEC standalone system under one sun illumination (11.5 mA cm⁻², Fig. 3c). Fig. 3d shows a photograph of H₂ production on a Pt electrode during the PEC measurement. Under our experimental conditions, a H₂ generation rate of ~10 mL cm⁻² per day was obtained for the LSC-PEC device (Fig. S7†), based on the J - t curve (Fig. 3e).¹² Considering that different light intensities are irradiated on the photoanode of the PEC and LSC-PEC systems, we investigated the dependence of the sunlight intensity on J . As shown in Fig. S8a and b,† as the sunlight intensity increases from 25 mW cm⁻² to 200 mW cm⁻², the J approximately increases linearly

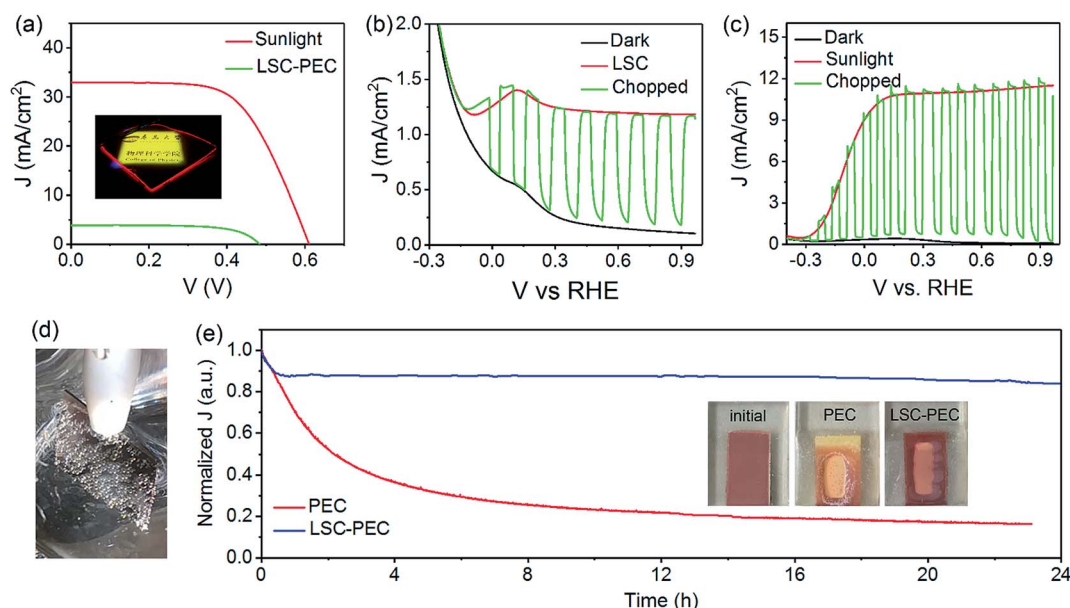


Fig. 3 (a) Solar cell J - V curves of a standalone solar cell (red line) and the same cell posited 2 cm away from one edge of the CdSe/CdS QD based LSC (equal to the position of the photoanode, green). The inset is the photograph of the LSC upon sunlight illumination. (b) and (c) J - V curves of the PEC device using the CdSe/CdSSe/CdS QDs-TiO₂ photoanode in the dark, under chopped and constant LSC illumination (11.8 mW cm⁻²) (b) or sunlight illumination (100 mW cm⁻²) (c). (d) Photograph of H₂ production on a Pt electrode. (e) Normalized J - t curves for the CdSe/CdSSe/CdS QDs-TiO₂ photoanode at 0.6 V vs. RHE under one sun illumination and LSC illumination. Insets are the photographs of the initial photoanode and photoanodes after 23 hours of one sun illumination in the PEC and LSC-PEC systems, respectively.

from 2.0 mA cm^{-2} to 9.0 mA cm^{-2} . Based on the dependence of the J on sunlight intensity, we can predict the relationship between the optical efficiency of LSCs and the H_2 generation efficiency of the PEC device. Taking a $10 \times 10 \times 0.2 \text{ cm}^3$ LSC as an example, when the η_{opt} of the LSC is higher than 9.3%, the J will be comparable to or even higher than that of the PEC standalone system. Further improvement of the solar-to- H_2 generation efficiency in the LSC-PEC system could be achieved by enhancing the η_{opt} of the LSC. At present, the η_{opt} of the LSC is up to 26% ($10 \times 10 \text{ cm}^2$) for perovskite based LSCs,³² which indicates that the LSC-PEC system represents a potential solution for achieving high efficiency PEC devices for H_2 production.

We further studied the stability of the PEC device by measuring the J as a function of time ($J-t$) under LSC illumination or sunlight illumination with an applied potential at 0.6 V vs. RHE. In order to give a reasonable comparison, the data of J are normalized by dividing the maximum value. Fig. 3e and Table 1 show the stability of the LSC-PEC system and the PEC standalone system under one sun illumination. For the PEC system, during PEC measurement, the temperature was slightly increased in first 1 h due to sunlight irradiation, and then remains at a relatively stable temperature ($\sim 24^\circ\text{C}$ for 100 mL electrolyte) (Fig. S9†). For the LSC-PEC system, the temperature does not show significant change ($\sim 18^\circ\text{C}$) due to the weak light intensity (11.8 mW cm^{-2}) emitted by the LSC. During the measurements, the η_{opt} of the LSC shows no significant changes, and the light intensity of the LSC radiating to the photoanode remains at $\sim 11.8 \text{ mW cm}^{-2}$. The two curves show a similar declining trend, initially dropping rapidly and then declining slowly. For the LSC-PEC system, the J declined sharply in the first 15 min, and then leveled off gradually with the increase of time. After 1 hour of continuous illumination by the LSC (11.8 mW cm^{-2}), the J of the PEC device dropped to 87.9% of its initial value. After 8 hours of LSC illumination, it maintained 87.6% of its initial value. While for the PEC standalone system, during the first 2 hours of illumination, the J dropped quickly and then the decline rate slowed down. After 2 hours of sunlight illumination (100 mW cm^{-2}), the J of the device dropped to 52.4% of its initial value, and then further decreased to 25.5% after 8 hours under one sun illumination. After long term continuous sunlight illumination (23 h), the J of the PEC standalone device dropped to 16.2% of its initial value, while for the LSC-PEC system, it remained at 84.6% of its initial value. The inset in Fig. 3e shows that the color of the photoanode after the 23 hours PEC operation fades away under sunlight illumination, while under LSC illumination, there is no obvious color change. These results indicate that the QDs in the PEC alone system may be oxidized, while the QDs in the LSC-

PEC system are quite stable. To better compare the stability of the PEC and LSC-PEC devices, we measured the $J-t$ curves of PEC devices under different sunlight intensities, as shown in Fig. S8c.† All the current densities show gradual decrease even at a lower light intensity. After 1 hour of sunlight illumination under 25, 60, 100 and 200 mW cm^{-2} (AM 1.5G), the J maintained 71%, 56%, 54%, and 49% of its value, respectively. This indicates that the stability of the PEC devices can be affected by the light intensity, especially at low light intensities. However, this finding cannot explain the stable J of the LSC-PEC system. To further understand the improved stability of the LSC-PEC system compared to the PEC system alone, we investigated the stability of the PEC devices by illuminating them at certain wavelengths.

After the light with wavelengths of $350 \pm 5 \text{ nm}$, $400 \pm 5 \text{ nm}$, $450 \pm 5 \text{ nm}$, $550 \pm 5 \text{ nm}$, $600 \pm 5 \text{ nm}$ and $700 \pm 5 \text{ nm}$ passes through the bandpass filter, the light intensity irradiated to the photoanodes is 1.6, 5.3, 6.0, 6.1, 5.8 and 5.1 mW cm^{-2} , respectively. As shown in Fig. 4a, the photoanode exhibits the highest J of $\sim 0.6 \text{ mA cm}^{-2}$ at $\sim 0.6 \text{ V}$ vs. RHE at a light wavelength of $550 \pm 5 \text{ nm}$ ($\sim 6.1 \text{ mW cm}^{-2}$). At light wavelengths of $400 \pm 5 \text{ nm}$, $450 \pm 5 \text{ nm}$ and $600 \pm 5 \text{ nm}$, the photocurrent densities per mW of light power were calculated to be 0.50, 0.52 and $0.45 \text{ mA cm}^{-2} \text{ mW}^{-1}$, respectively (Fig. 4b). The J of the photoanode shows a weak photoresponse upon illumination with $700 \pm 5 \text{ nm}$ light, due to the very weak absorption of the QDs. The $J-t$ curves show that the stability of the PEC devices is associated with the light wavelength (under different light wavelengths). As shown in Fig. 4c, the QD based photoanodes under illumination with light of $450 \pm 5 \text{ nm}$, $550 \pm 5 \text{ nm}$ and $600 \pm 5 \text{ nm}$ wavelength have better stability compared with UV light illumination ($350 \pm 5 \text{ nm}$ and $400 \pm 5 \text{ nm}$). Under illumination with a light of wavelength $550 \pm 5 \text{ nm}$, the PEC devices have the highest stability and the J retained 76.5% of its initial value after 1 hour of illumination. In contrast, under UV light illumination ($350 \pm 5 \text{ nm}$ and $400 \pm 5 \text{ nm}$), especially for light of $400 \pm 5 \text{ nm}$ wavelength, the J of the devices decreased to 47.3% of its initial value after 1 hour of continuous illumination. This indicates that UV light radiation may cause severe damage to the QDs and could result in serious decline in the stability of the QD based PEC devices.³⁹ For the TiO_2 -QD photoanodes, UV light induces the degradation of the QDs and excess holes of TiO_2 , leading to the interaction between the QDs and the photoinduced holes in TiO_2 , which decreases not only the charge transfer rate, but also the current density, further affecting the stability of the PEC devices.³⁹ Thus, besides the light intensity, UV light is another factor inducing the continuous drop of J . The efficiency and stability of the PEC system with a long pass filter (400–780 nm) were measured for

Table 1 The percentage of remaining J for the PEC standalone and LSC-PEC system after irradiation for a certain time under sunlight illumination of 100 mW cm^{-2}

Devices	0.5 h	1 h	2 h	4 h	6 h	8 h	12 h	16 h	20 h	23 h
PEC	84.9%	70.6%	52.4%	36.4%	29.4%	25.5%	21.7%	19.0%	17.3%	16.2%
LSC-PEC	88.7%	87.9%	87.8%	87.6%	87.6%	87.6%	87.4%	87.3%	85.9%	84.6%

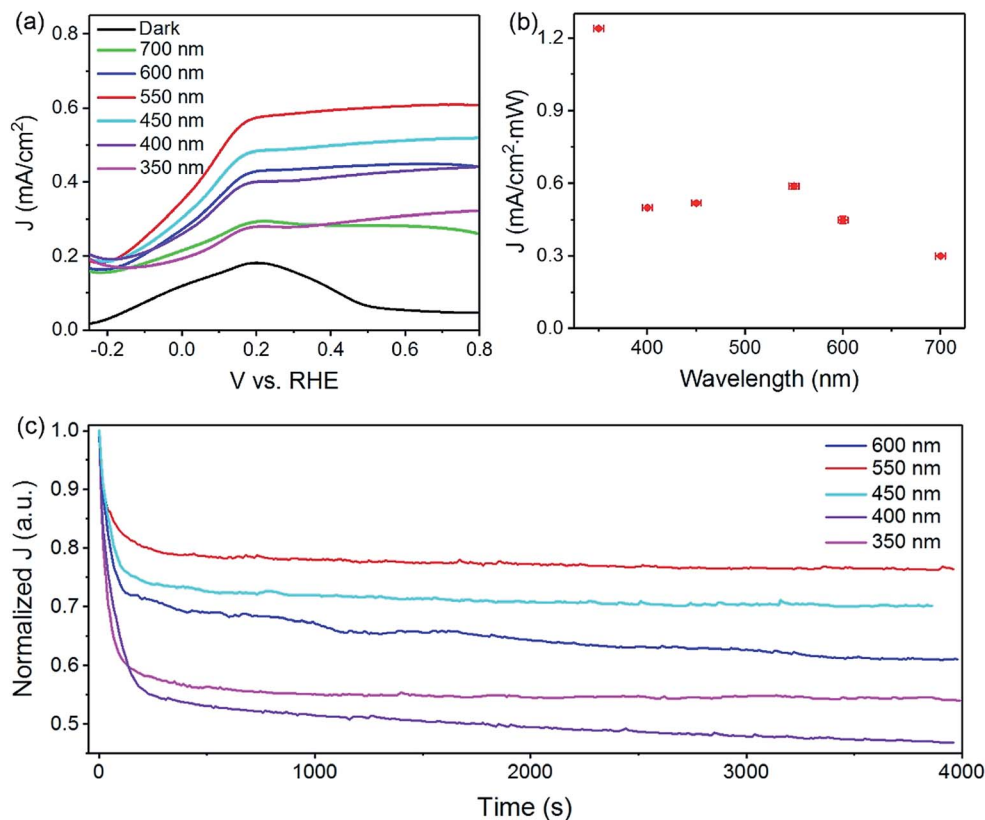


Fig. 4 (a) J - V curves of the PEC device using the CdSe/CdSSe/CdS QDs-TiO₂ photoanode in the dark and under illumination with different bandpass filters (bandwidth of 10 nm). (b) J per energy vs. the sunlight wavelength. (c) Normalized J - t at 0.6 V vs. RHE under illumination with different bandpass filters.

comparison with those of the PEC system without a filter, as shown in Fig. S10.† This long pass filter can block sunlight with wavelengths shorter than 400 nm and longer than 780 nm. When a pristine PEC device with a filter is used, the initial efficiency is lower than that for the PEC system without a filter, but the stability of the PEC standalone system is enhanced. This result indicates the side effect of UV light on the stability of the PEC device and even the filter cannot fully remove UV light in the wavelength region of 400–450 nm. These findings further confirm that the combination of an LSC with PEC devices is an effective way to improve the stability of PEC devices by converting UV light to visible light.

Usually, the corrosion of QDs due to strong alkalinity (electrolyte, pH \sim 13) can reduce the stability of PEC devices. The stability of the photoanodes was investigated under one sun illumination (100 mW cm^{-2}) in 0.2 M Na₂SO₄ (pH \sim 7) aqueous solution, as shown in Fig. S11.† The J of the PEC system is \sim 0.8 mA cm⁻² at 0.6 V vs. RHE, and after 30 minutes of continuous illumination, it quickly dropped to \sim 27% of its initial value. As there is no hole scavenger in this electrolyte, the slow hole reaction induces not only fast e-h recombination, but also hole accumulation, explaining the low J and bad stability, respectively. In fact, the result clearly indicates that the first quick-drop of J (initial 15 min) in PEC devices using S²⁻/SO₃²⁻ as the electrolyte is mainly due to the hole accumulation of QDs. For the PEC standalone system, the photoanode was exposed to

sunlight (280–4000 nm). Due to the activation of UV light, the holes of TiO₂ react with QDs leading to photo-oxidation; meanwhile UV light induces the degradation of QDs, which leads to the continuous drop of J . However, for the LSC-PEC system, the photoanode was irradiated under visible light (570–670 nm). When the holes accumulate to a certain extent, the accumulative effect tends to be stable and the device remains stable after the first quick-drop of J .

In addition to improving the stability of the PEC devices, another motivation for developing a LSC-PEC system is the potential for the reduction in cost of H₂ generation. We estimated the cost of a 1 m \times 1 m \times 0.8 cm LSC-PEC device (photoanode attached to the four edges of the LSC), and performed a comparison with the cost for the PEC standalone device under the same H₂ yield (mol per day, ESI Tables S1–S7†). Based on our analysis, the cost of 1 m² LSC coupled with 320 cm² PEC device is \$23.42. When the η_{opt} of the LSC reaches 8% (already reported in the literature ref. 40), the cost of the LSC-PEC device can be comparable to the PEC standalone device (ESI Table S6†). Considering the 420% improvement in stability for the LSC-PEC device (Fig. 3e), when the η_{opt} of the LSC is 4.5%, the cost of the LSC-PEC composite system is equivalent to the PEC single system (ESI Table S7†). If the η_{opt} of the LSC improves to 8%, the maximum cost saving can be increased to \sim 49%.

In the above LSC-PEC system, the long distance between the LSC and photoanode (2 cm) limits the light intensity radiating

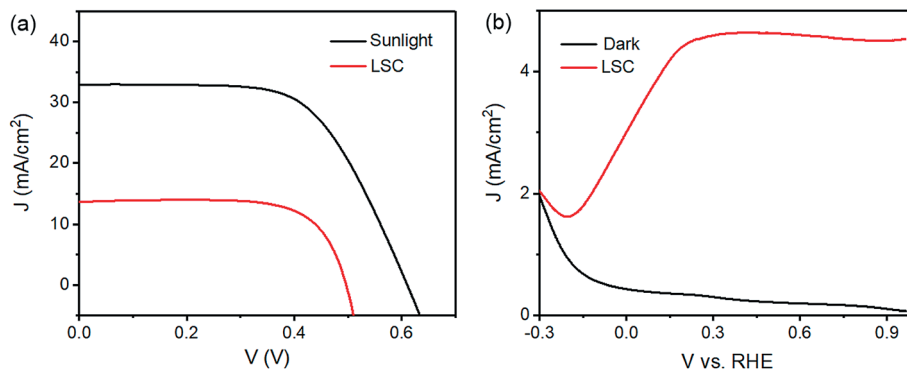


Fig. 5 (a) Solar cell J - V curves of a standalone solar cell and the same cell posited 0.2 cm away from one edge of the CdSe/CdS QD based LSC (equal to the position of the photoanode). (b) J - V curves of the PEC device using the CdSe/CdS/CdS QDs-TiO₂ photoanode in the dark and under constant LSC illumination (42.6 mW cm⁻²).

to the photoanode, which leads to the waste of the emitted photons from the LSC. We further regulated the geometry of the system by changing the electrolytic tank from cylindrical glass to square quartz to decrease the distance between the LSC and photoanode (Fig. S12[†]), which directly increases the light power illuminated on the photoanode and further enhances the H₂ generation efficiency. As shown in Fig. 5a, the light intensity radiating to the photoanode surface increased to 42.6 mW cm⁻² under natural sunlight illumination (82 mW cm⁻²), and the J of the LSC-PEC system increased to 4.5 mA cm⁻² at ~0.6 V vs. RHE (Fig. 5b), which are comparable to previous reports (Table S8[†]). In addition, the CdSe/CdS/CdS QDs can absorb light at a wavelength of 300–650 nm, and their absorption at a shorter wavelength is indeed stronger. To well match the spectra between LSC emission and PEC absorption, carbon dots (C-dots) were further used to prepare an LSC, which emit at a wavelength of 450–650 nm (Fig. S13a[†]). The C-dot based LSC was prepared by drop casting a C-dots/polyvinyl-pyrrolidone polymer mixture in methanol.³⁸ The η_{opt} of the LSC is measured to be 4.7% (Fig. S13b[†]), and the J of the LSC-PEC system is 3.8 mA cm⁻² at ~0.6 V vs. RHE (Fig. S13c[†]) which is lower than that in the CdSe/CdS QD based LSC-PEC system due to the lower η_{opt} of the C-dot based LSC. To further improve the efficiency of the LSC-PEC device, one can optimize the overlap of the emission spectrum of the LSC and the absorption spectrum of the anode, besides the improvement of the efficiency of the LSC or PEC itself. For example, the maximum η_{opt} of the core/shell QD based LSC was 8.1% with CuInS₂/ZnS QDs whose emission spectrum ranges from 730 nm to 1100 nm.⁴⁰ One should develop a near-infrared QD based photoanode with absorption in the range of 730–1100 nm, so as to match the emission spectrum of the LSC to improve the stability and H₂ generation efficiency of PEC devices. In addition, an external bias is still needed in the PEC system, while LSCs can couple with solar cells to realize photoelectric conversion (Fig. 1a), which can be used to provide the needed bias for H₂ generation. Therefore, it is possible to fabricate a PEC system for H₂ generation using solar radiation as the only energy source by integrating the PEC device with an LSC and solar cells into a standalone system.

Conclusions

In conclusion, we proposed the concept of integrating a PEC device with an LSC to improve the stability of H₂ generation. CdSe/CdS/CdS QDs were used as a photosensitizer in the PEC device. A CdSe/CdS QD based LSC was introduced to convert UV light to visible light that can be absorbed by the PEC device. In the LSC-PEC system, a saturated photocurrent density of 1.2 mA cm⁻² is achieved, and 84.6% of it was maintained after 23 hours of continuous illumination. This shows a drastic increase in stability compared to a similar PEC device without the LSC part. In addition, the combination of the LSC and the PEC device can reduce the cost of H₂ generation when the optical efficiency of the LSC is high enough (ideally, >4.5%). Further integration of the LSC-PEC device with a solar cell into a standalone system will achieve stable PEC H₂ generation by energy self-sufficiency without an external bias.

Experimental section

Device fabrication

The LSC was prepared by embedding QDs in a polymer matrix. Typically, CdSe/CdS QDs (50 mg) dispersed in toluene were added to a 50 mL flask and the solvent was pumped away. The monomer precursors lauryl methacrylate (LMA) and ethylene glycol dimethacrylate (EGDM) were mixed at a mass ratio of 5.5 : 1. Then the solution mixture was mixed with a UV initiator (diphenyl(2,4,6-trimethylbenzoyl)phosphine oxide) and ultrasonically treated until a clear solution (5 mL) was obtained. The solution was then transferred into the flask and mixed with CdSe/CdS QDs. Then the mixture was injected into a model consisting of two glass slides separated by a flexible silicon rubber spacer with a thickness of ~2 mm. Finally, the mixture was kept under UV illumination for 2 hours.

The QD based photoanode was prepared by EPD. Briefly, FTO glass substrates were cleaned with acetone, ethanol and water sequentially and dried under a N₂ flow. A TiO₂ blocking layer was spin coated on the FTO substrates at a speed of 5000 rpm for 30 s by using a commercial Ti-nanoxide solution. Then the films were annealed in air at 500 °C for 30 min and cooled

down to room temperature. Subsequently, a commercial TiO₂ paste was deposited on the TiO₂ coated FTO substrates by tape casting and dried in air for 15 min. The photoanodes were then heated on a hot plate at 120 °C for 6 min, and finally annealed according to the following temperature profile: 325 °C for 5 min, 375 °C for 5 min, 450 °C for 15 min and 500 °C for 30 min with a heating rate of 10 °C min⁻¹. In the end, two TiO₂ films were vertically immersed in the QD toluene solution, facing each other with a distance of 0.8 cm and a direct bias of 210 V for 90 min. Then the photoanodes were rinsed with toluene and dried with N₂ at room temperature. Finally, two coating cycles of ZnS layers were applied by dipping into 0.1 M Zn(Ac)₂ and 0.1 M Na₂S solutions for 1 min alternately.

Optical measurements of the LSCs

The optical efficiency of the LSC based on CdSe/CdS QDs was measured by using a solar simulator (94011A LCS-100 solar simulator, Newport). The spectrum intensity was measured using an optical power meter (Newport Model 843-R). The *J-V* curves were measured using a Keithley 2400 source meter under simulated sunlight. During measurements, a standard photovoltaic cell was directly coupled at one side of LSC edges using a reflective mirror below the LSC.

PEC measurements of photoanodes

A typical three-electrode system consisting of a QDs-TiO₂ working electrode, Pt counter electrode and saturated Ag/AgCl reference electrode was used to investigate the PEC performance. An aqueous solution containing 0.25 M Na₂S and 0.35 M Na₂SO₃ was used as the electrolyte to trap holes (pH ~ 13). For comparison, a 0.2 M Na₂SO₄ (pH ~ 7) aqueous solution was also used as the electrolyte to study the effect of the S²⁻/SO₃²⁻ electrolyte. All measured potentials were converted to the potentials vs. RHE according to the following equation: $V_{\text{RHE}} = V_{\text{Ag/AgCl}} + 0.1976 + 0.059 \times \text{pH}$. *J-V* curves were measured using an electrochemical workstation (Autolab, PGSTAT 302N) under light emission by the LSC or simulated sunlight using a LCS-100 solar simulator (100 mW cm⁻²). The working area of the QDs-TiO₂ photoanode was 0.1–0.4 cm². All PEC devices were measured at room temperature in winter (~10 °C).

The synthesis of the QDs and their characterization are described in the ESI.†

Conflicts of interest

The authors declare no conflict of interest.

Acknowledgements

H. G. Zhao acknowledges the funding from the Natural Science Foundation of Shandong Province (ZR2018MB001) and the start-up funding support from Qingdao University. Y. Q. Wang would like to acknowledge the financial support from the Top-notch Innovative Talent Program of Qingdao City (Grant No. 13-CX-8) and the Qingdao International Center for Semiconductor

Photoelectric Nanomaterials, and the Shandong Provincial University Key Laboratory of Optoelectrical Material Physics and Devices.

References

- 1 T. Leijtens, K. A. Bush, R. Prasanna and M. D. McGehee, *Nat. Energy*, 2018, **3**, 828–838.
- 2 H. Li, K. Wu, J. Lim, H. J. Song and V. I. Klimov, *Nat. Energy*, 2016, **1**, 16157.
- 3 A. Fujishima and K. Honda, *Nature*, 1972, **238**, 37–38.
- 4 M. Grätzel, *Nature*, 2001, **414**, 338–344.
- 5 J. Qi, W. Zhang and R. Cao, *Adv. Energy Mater.*, 2018, **8**, 1701620.
- 6 Z. Zhou, Z. Wu, Q. Xu and G. Zhao, *J. Mater. Chem. A*, 2017, **5**, 25450–25459.
- 7 W. K. Bae, Y. S. Park, J. Lim, D. Lee, L. A. Padilha, H. McDaniel, I. Robel, C. Lee, J. M. Pietryga and V. I. Klimov, *Nat. Commun.*, 2013, **4**, 2661.
- 8 Y. Yan, R. W. Crisp, J. Gu, B. D. Chernomordik, G. F. Pach, A. R. Marshall, J. A. Turner and M. C. Beard, *Nat. Energy*, 2017, **2**, 17052.
- 9 R. Adhikari, K. Basu, Y. Zhou, F. Vetrone, D. Ma, S. Sun, F. Vidal, H. Zhao and F. Rosei, *J. Mater. Chem. A*, 2018, **6**, 6822–6829.
- 10 P. Rodenas, T. Song, P. Sudhagar, G. Marzari, H. Han, L. Badia-Bou, S. Gimenez, F. Fabregat-Santiago, I. Mora-Sero, J. Bisquert, U. Paik and Y. S. Kang, *Adv. Energy Mater.*, 2013, **3**, 176–182.
- 11 R. Trevisan, P. Rodenas, V. Gonzalez-Pedro, C. Sima, R. S. Sanchez, E. M. Barea, I. Mora-Sero, F. Fabregat-Santiago and S. Gimenez, *J. Phys. Chem. Lett.*, 2013, **4**, 141–146.
- 12 G. Liu, Z. Ling, Y. Wang and H. Zhao, *Int. J. Hydrogen Energy*, 2018, **43**, 22064–22074.
- 13 Y. Bu, Z. Chen, W. Li and J. Yu, *ACS Appl. Mater. Interfaces*, 2013, **5**, 5097–5104.
- 14 M. Y. Huang, X. B. Li, Y. J. Gao, J. Li, H. L. Wu, L. P. Zhang, C. H. Tung and L. Z. Wu, *J. Mater. Chem. A*, 2018, **6**, 6015–6021.
- 15 Y. Liu, R. Li, P. Gao, Y. Zhang, H. Ma, J. Yang, B. Du and Q. Wei, *Biosens. Bioelectron.*, 2015, **65**, 97–102.
- 16 W. Li and F. Jäckel, *Nanoscale*, 2018, **10**, 16153–16158.
- 17 P. Wang, M. Wang, J. Zhang, C. Li, X. Xu and Y. Jin, *ACS Appl. Mater. Interfaces*, 2017, **9**, 35712–35720.
- 18 J. Y. Kim, Y. J. Jang, J. Park, J. Kim, J. S. Kang, D. Y. Chung, Y. E. Sung, C. Lee, J. S. Lee and M. J. Ko, *Appl. Catal., B*, 2018, **227**, 409–417.
- 19 F. Su, J. Lu, Y. Tian, X. Ma and J. Gong, *Phys. Chem. Chem. Phys.*, 2013, **15**, 12026–12032.
- 20 L. Etgar, D. Yanover, R. K. Čapek, R. Vaxenburg, Z. Xue, B. Liu, M. K. Nazeeruddin, E. Lifshitz and M. Grätzel, *Adv. Funct. Mater.*, 2013, **23**, 2736–2741.
- 21 M. Cirillo, T. Aubert, R. Gomes, R. Van Deun, P. Emplit, A. Biermann, H. Lange, C. Thomsen, E. Brainis and Z. Hens, *Chem. Mater.*, 2014, **26**, 1154–1160.

- 22 S. Brovelli, W. K. Bae, C. Galland, U. Giovanella, F. Meinardi and V. I. Klimov, *Nano Lett.*, 2014, **14**, 486–494.
- 23 T. Leijtens, G. E. Eperon, S. Pathak, A. Abate, M. M. Lee and H. J. Snaith, *Nat. Commun.*, 2013, **4**, 2885.
- 24 R. Asahi, T. Morikawa, T. Ohwaki and Y. Taga, *Science*, 2001, **293**, 269–271.
- 25 F. Meinardi, A. Colombo, K. A. Velizhanin, R. Simonutti, M. Lorenzon, L. Beverina, R. Viswanatha, V. I. Klimov and S. Brovelli, *Nat. Photonics*, 2014, **8**, 392–399.
- 26 R. Mazzaro and A. Vomiero, *Adv. Energy Mater.*, 2018, **8**, 1801903.
- 27 Y. Zhou, H. Zhao, D. Ma and F. Rosei, *Chem. Soc. Rev.*, 2018, **47**, 5866–5890.
- 28 S. Sadeghi, H. B. Jalali, R. Melikov, B. G. Kumar, M. M. Aria, C. W. Ow-Yang and S. Nizamoglu, *ACS Appl. Mater. Interfaces*, 2018, **10**, 12975–12982.
- 29 H. Liu, S. Li, W. Chen, D. Wang, C. Li, D. Wu, J. Hao, Z. Zhou, X. Wang and K. Wang, *Sol. Energy Mater. Sol. Cells*, 2018, **179**, 380–385.
- 30 J. A. H. P. Sol, V. Dehm, R. Hecht, F. Würthner, A. P. H. J. Schenning and M. G. Debije, *Angew. Chem., Int. Ed.*, 2018, **57**, 1030–1033.
- 31 Y. You, X. Tong, W. Wang, J. Sun, P. Yu, H. Ji, X. Niu and Z. M. Wang, *Adv. Sci.*, 2019, **6**, 1801967.
- 32 M. Wei, F. P. G. de Arquer, G. Walters, Z. Yang, L. N. Quan, Y. Kim, R. Sabatini, R. Quintero-Bermudez, L. Gao, J. Z. Fan, F. Fan, A. Gold-Parker, M. F. Toney and E. H. Sargent, *Nat. Energy*, 2019, **4**, 197–205.
- 33 K. Wu, H. Li and V. I. Klimov, *Nat. Photonics*, 2018, **12**, 105–110.
- 34 D. Cambié, F. Zhao, V. Hessel, M. G. Debije and T. Noël, *Angew. Chem., Int. Ed.*, 2017, **56**, 1050–1054.
- 35 B. Mahler, N. Lequeux and B. Dubertret, *J. Am. Chem. Soc.*, 2010, **132**, 953–959.
- 36 M. Zhu, Y. Li, S. Tian, Y. Xie, X. Zhao and X. Gong, *J. Colloid Interface Sci.*, 2019, **534**, 509–517.
- 37 X. Gong, W. Ma, Y. Li, L. Zhong, W. Li and X. Zhao, *Org. Electron.*, 2018, **63**, 237–243.
- 38 G. Liu, H. Zhao, F. Diao, Z. Ling and Y. Wang, *J. Mater. Chem. C*, 2018, **6**, 10059–10066.
- 39 M. R. Bergren, N. S. Makarov, K. Ramasamy, A. Jackson, R. Guglielmetti and H. McDaniel, *ACS Energy Lett.*, 2018, **3**, 520–525.
- 40 K. Basu, H. Zhang, H. Zhao, S. Bhattacharya, F. Navarro-Pardo, P. K. Datta, L. Jin, S. Sun, F. Vetrone and F. Rosei, *Nanoscale*, 2018, **10**, 15273–15284.